CrossMark

High-speed OH* chemiluminescence imaging of ignition through a shock tube end-wall

V. A. Troutman[1] · C. L. Strand[1] · M. F. Campbell[2] · A. M. Tulgestke[1] · V. A. Miller[1] ·
D. F. Davidson[1] · R. K. Hanson[1]

Abstract A high-speed OH* chemiluminescence imaging diagnostic was developed to image the structure and homogeneity of combustion events behind reflected shock waves in the Stanford Constrained Reaction Volume Shock Tube. An intensified high-repetition-rate imaging system was used to acquire images of OH* chemiluminescence (near 308 nm) through a fused quartz shock tube end-wall window at 10–33 kHz during the combustion of n-heptane (21 % O_2/Ar, $\phi = 0.5$). In general, the imaging technique enabled observation of the main ignition event in the core of the shock tube that corresponded to typical markers of ignition (e.g., pressure rise), as well as localized ignition near the wall that preceded the main core ignition event for some conditions. Case studies were performed to illustrate the utility of this novel imaging diagnostic. First, by comparing localized wall ignition events to the core ignition event, the temperature homogeneity of the post-reflected shock gas near the end-wall was estimated to be within 0.5 % for the test condition presented ($T = 1159$ K, $P = 0.25$ MPa). Second, the effect of a recession in the shock tube wall, created by an observation window, on the combustion event was visualized. Localized ignition was observed near the window, but this disturbance did not propagate to the core of the shock tube before the main ignition event. Third, the effect of shock tube cleanliness was investigated by conducting tests in which the shock tube was not cleaned for multiple consecutive runs. For tests after no cleaning was performed, ignition events were concentrated in the lower half of the shock tube. In contrast, when the shock tube was cleaned, the ignition event was distributed around the entire circumference of the shock tube; validating the cleaning procedure.

1 Introduction

Shock tubes have been used for over 60 years in a wide range of experimental capacities, including the investigation of chemical kinetics over large spans of temperature and pressure [1]. Traditionally, insight into the temperature, pressure and species concentrations in the shock tube is gained through diagnostics that are positioned at ports machined into the side-wall of the test section. For instance, pressure transducers and windows for observing path-integrated light emission or absorption can be positioned at these port locations [2]. While these diagnostics have proven to be valuable, they cannot provide spatial (radial) information regarding the structure and homogeneity of the test gas. A particular need not met by traditional diagnostics is to understand the facility-specific uniformity of the reflected shock reaction volume for exothermic (combusting) mixtures to allow valid comparison of experimental results with chemical kinetics models that assume homogeneous conditions. There are many potential causes of non-uniformity within the shock tube, including non-ideal fluid flow, reflected shock bifurcation and wall heat transfer, though these effects are generally neglected in modeling reflected shock ignition.
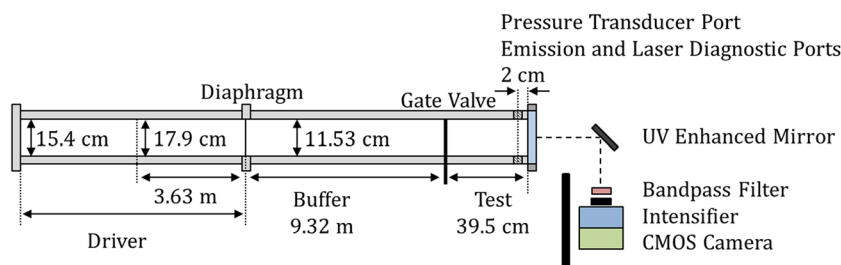
✉ V. A. Troutman
vtrout@stanford.edu

1 High Temperature Gasdynamics Laboratory, Stanford University, Stanford, CA, USA

2 Combustion Research Facility, Sandia National Laboratory, Livermore, CA, USA

Fig. 1 The dimensions of the Stanford Constrained Reaction Volume Shock Tube (CRVST) and the configuration of the imaging system are shown

Previous combustion imaging studies in shock tubes have utilized multiple techniques. In early work, Vermeer et al. [3] used schlieren to image the ignition process of hydrocarbons near the end-wall in a rectangular shock tube. Fieweger et al. [4] used shadowgraph to visualize the auto-ignition of several fuels in a square shock tube with transparent side-walls next to the end-wall. Herzler et al. [5] collected a single visible-emission image shortly after the ignition event of propane through a small window in the center of the end-wall of a shock tube. Penyazkov et al. [6] mounted two ($D = 8$ mm) quartz rods into the end-wall to collect emission (OH, CH and C_2 radicals) data simultaneously in the boundary layer and the center of a shock tube for ethylene auto-ignition. More recently, Heufer and Olivier [7] performed schlieren imaging in a rectangular shock tube to investigate biofuel combustion.

Other previous imaging techniques of note investigated various phenomena in shock tubes and similar experimental facilities. Yoo et al. [8] performed toluene PLIF through the side-wall of a shock tube using a transparent and square test section attachment to visualize the flow field and measure the temperature field in non-reactive mixtures at relatively low temperatures. Wegener et al. [9] obtained holographic recordings of the diaphragm rupturing in an expansion tube through optical ports in the wall. In related work, Mansfield et al. [10] used a transparent end-wall in a rapid compression facility to image the ignition process and determine the existence of both inhomogeneous and homogeneous auto-ignition. These imaging studies are akin to imaging in an optically accessible engine, where an understanding of the engine operation can be garnered from watching the combustion process unfold inside the engine cylinder. For example, Stojkovic et al. [11] implemented high-speed OH* chemiluminescence in an engine through a window located in the piston to study soot formation and oxidation.

In the current work, OH* chemiluminescence, a common emission diagnostic for combustion systems, was used as a qualitative marker of the reaction zone. OH* chemiluminescence (peak emission occurring near 308 nm) was used to indicate the locations of high radical concentrations [12, 13]. With emission in the UV, OH* chemiluminescence was easily studied with very little ambient light contamination by using a band-pass filter.

Here, combustion events in a shock tube were imaged through a UV-transparent (fused quartz) end-wall with a high-repetition-rate intensified camera. The resulting collected images were axially integrated emission indicating the spatial location and geometry of the ignition event. In this work, the reaction volume was constrained to a small portion of the end-wall (see Sect. 2.1 for details), which drastically limited the length of the integration path. For potentially long axial integration paths (e.g., conventional shock tubes), greater care would need to be taken. In general, chemiluminescence images must be interpreted with caution because they are integrated measurements, but they yield powerful information otherwise unavailable from traditional diagnostics through side-wall ports [14].

Through this work, an improved understanding of shock tube performance and diagnostics was sought. Three case studies that illustrate the utility of this imaging diagnostic were performed: Temperature Homogeneity (Sect. 3.1), Shock Tube Wall Defects (Sect. 3.2), and Shock Tube Cleanliness (Sect. 3.3).

2 End-wall imaging system design

2.1 Stanford Constrained Reaction Volume Shock Tube

The Stanford Constrained Reaction Volume Shock Tube (CRVST), as shown schematically in Fig. 1, was developed to study the kinetics of low-vapor-pressure fuels [15]. The internal diameter of the buffer and test sections is 11.53 cm, and these sections contribute to 9.7 m of the shock tube length. The driver section, with a length of 3.63 m, has an internal diameter of 17.9 cm. A driver extension piece increases the driver section length to a maximum of 13.42 m and has an internal diameter of 15.4 cm (further detailed information regarding the CRVST, the driver section and driver inserts can be found in [16]). Located 2 cm away from the end-wall, machined ports are situated that house windows for laser or emission diagnostics and other sensors such as pressure transducers.

The shock tube was run in constrained reaction volume (CRV) mode. CRV mode employed a sliding gate valve to mechanically confine the reactive gas mixture to a small

Fig. 2 The four-piece transparent end-wall window design allows spatial imaging of the ignition event behind a reflected shock wave through the end-wall of the Stanford CRVST
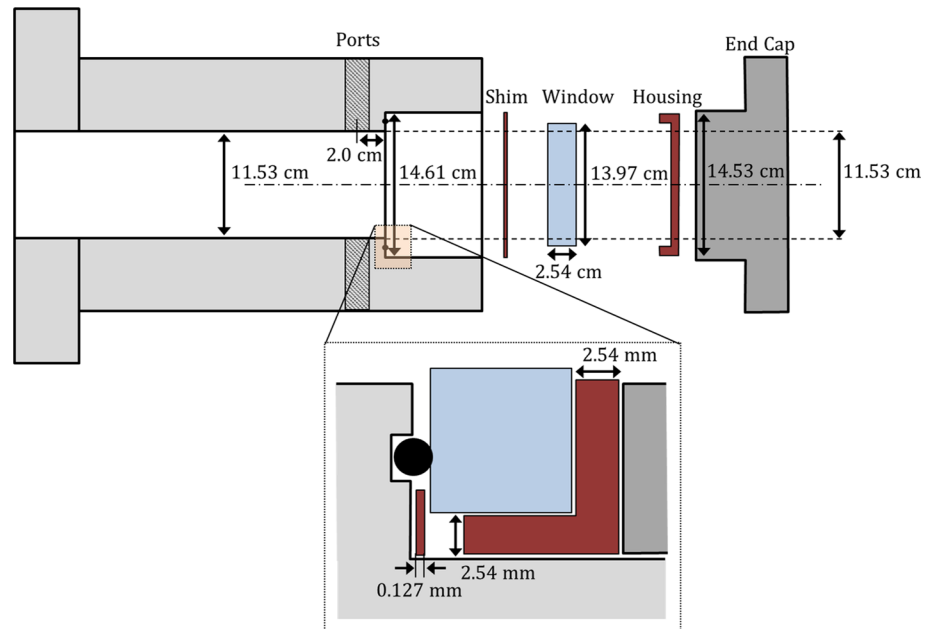
fraction of the shock tube length, near the end-wall [15]. This gate valve was opened just before the shock wave was initiated, i.e., when the Lexan diaphragm burst, in order to minimize the dilution of the test gas mixture. The axial extent of the test gas after the reflected shock, L_5, ranged from 5 to 10 cm for the conditions studied [17].

For each experiment, the driver section was filled with a tailored helium and nitrogen mixture. The buffer section contained a tailored mixture of carbon dioxide, nitrogen and argon (see Refs. [15, 16] for driver and buffer gas tailoring details). For all tests presented here, the test section was filled with normal heptane, oxygen and argon, at an equivalence ratio of $\phi = 0.5$. Research-grade helium, nitrogen, carbon dioxide, argon and oxygen were obtained from Praxair, Inc., and spectroscopic-grade normal heptane from Sigma-Aldrich was used. Test gas mixture compositions were determined via partial pressures in a mixing tank. Best practices previously developed to minimize the effect of mixing of the test gas and buffer gas were followed [17].

Initial test gas conditions (behind the reflected shock wave) were calculated from the speed of the incident shock wave, determined using the time-of-arrival technique via seven side-wall pressure transducers (PCB-113A26) distributed over the last section of the shock tube. Time zero for the experiment was defined at the half-rise of a Kistler (603B1) pressure transducer signal for the pressure jump due to the reflected shock wave. This pressure transducer was located 2 cm from the end-wall and was covered in room-temperature vulcanizing silicone (RTV). For reference, the time difference between the incident shock arrival at the end-wall and the passage of the reflected shock by the pressure transducer at 2 cm was typically $70\,\mu s$ and

varies slightly with initial conditions. Additionally, a traditional OH* emission diagnostic at 2 cm from the end-wall was implemented using a focusing lens, slit, UG-5 Schott Glass band-pass filter and a silicon photodetector (Thor-Labs PDA36A). Signals from the pressure transducers and emission detector were acquired at 10 MHz using a Lab-VIEW data acquisition system.

Initial reflected shock temperatures for this work ranged from 1057 to 1240 K. Initial reflected shock pressures ranged from 0.25 to 0.81 MPa.

2.2 End-wall window

The transparent end-wall window, as shown in Fig. 2, consists of four pieces: shim, window, housing and end cap. The window is a 13.97 cm (5.5 in.) diameter, 2.54 cm (1 in.) thick cylinder. In this work, a fused quartz window (GM Associates) transmits the 308 nm OH* chemiluminescence. This easily removable window is a critical design feature, as it allows cleaning of the window with acetone between experiments. The design also does not require any RTV or sealant, further aiding in the ease of window removal and re-installation. The window is rated for a maximum pressure of 2.4 MPa (safety factor of 4). An important feature of this end-wall window design is that it allows optical access out to the edge of the shock tube wall.

The Teflon shim is 0.127 mm (0.005 in.) thick and prevents over-tightening of the shock tube end cap. It allows the shock tube to be adequately sealed, while preventing excessive compressive stress on the window that can cause cracks. The 2.54 mm (0.1 in.) thick Teflon housing holds the window and protects the back of the window from

contact with the metal of the shock tube end cap. The end cap interior is hollow and is attached to the test section of the shock tube using four bolts.

2.3 Imaging system

A Vision Research Phantom v710 high-speed CMOS camera coupled to an intensifier was used to collect the OH* chemiluminescence. The intensifier was a LaVision HS-IRO equipped with a gen II S20 photocathode. A Sodern UV lens, with a focal length of $f = 100$ mm, was used with the aperture set to $f/4$ for all cases. To filter out stray light and other emission, an Asahi Spectra high-transmission band-pass filter centered at 313 nm with 10 nm FWHM was used.

In the interest of protecting the camera and intensifier in the event of a window or end cap failure, a UV-enhanced mirror was used to position the camera at a 90° angle to the shock tube (Fig. 1). Additionally, a shield was placed between the shock tube and camera.

For the v710 camera, there is a trade-off between image resolution (height × width pixels) and acquisition rate; a smaller window of pixels enables a faster acquisition rate. To allow the full shock tube cross section to be imaged at a faster rate, the camera was moved farther away from the shock tube. In this study, resolutions were used that range from 448×376 to 880×800 pixels, corresponding to acquisition rates of 33–10 kHz (inter-frame times ranging from 0.03 to 0.1 ms), respectively.

For the highest resolution, the projected pixel size was 6.59 pixels/mm (0.15 mm/pixel). For the lowest resolution, the projected pixel size was 3.26 pixels/mm (0.31mm/pixel). The depth of field for the 10 kHz setup was around 13 cm and for the 33 kHz setup was around 110 cm, both captured the full depth of the compressed test gas section ($L_5 = 5$ cm). The system was focused at the location of the diagnostic ports, 2 cm from the end-wall.

The intensifier was gated to 4 or 5 μs. The intensifier gain was adjusted specifically to visualize the locations of the earliest flames with 25–50 % of the maximum possible camera signal level. In this work, the gain was typically set at 50–60 % of the maximum gain setting.

3 Results and case studies

3.1 Temperature homogeneity

In a typical shock tube auto-ignition experiment, it is assumed that the test gas is uniformly heated by the reflected shock wave and rapid reaction occurs homogeneously throughout the reactor volume at the ignition delay time (IDT). The collected Kistler pressure transducer (2 cm
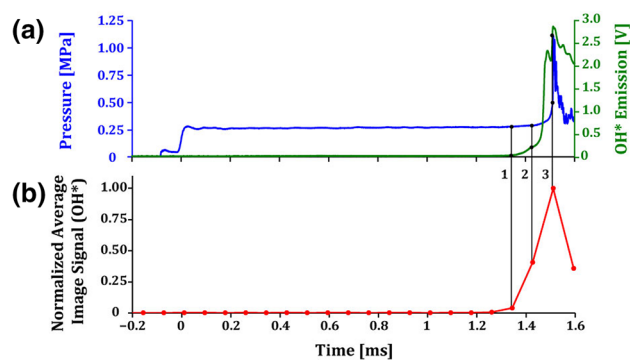

Fig. 3 **a** The pressure trace from the Kistler pressure transducer and voltage from the OH* emission detector (2 cm from the end-wall) of the combustion of *n*-heptane (21 % O_2/Ar, $\phi = 0.5$) are shown. The initial reflected shock conditions were 1159 K and 0.25 MPa. **b** The normalized spatially averaged signal from the collected end-wall images is shown. The images were recorded at 12 kHz with 5 μs exposure time. The *solid vertical bars* were numbered corresponding to the timing of the images shown in Fig. 4
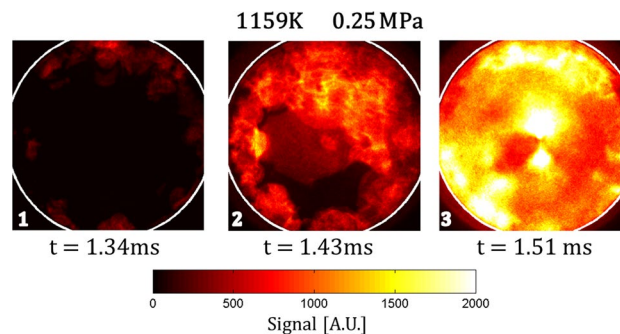

Fig. 4 The combustion of *n*-heptane (21 % O_2/Ar, $\phi = 0.5$) with initial reflected shock conditions of 1159 K and 0.25 MPa was recorded at 12 kHz with 5 μs exposure time. A *white outline* was included to mark the location of the shock tube wall. The timing of the three images was also indicated in Fig. 3

from the end-wall) signal is shown in Fig. 3a. The first rise in pressure (near $t = -0.1$ ms) is due to the incident shock wave passing over the pressure transducer and the second rise ($t = 0$ ms) is due to the reflected shock wave. The subsequent large "spike" in pressure (near $t = 1.5$ ms) corresponds to the ignition event and is representative of how IDT may be measured. Small changes in the pressure transducer signal or emission diagnostic, prior to the dramatic increase in pressure, are observed under some conditions and may be taken as evidence of partial inhomogeneity in the ignition event that needs to be better understood.

This imaging technique revealed the spatial distribution of ignition events that occured in the shock tube as they evolved in time. By acquiring a time series of images, the variability and hence the uncertainty in the IDT were quantified. Uncertainty in measuring the IDT is an often discussed

topic due to multiple choices of definitions, ignition indicators, and a large variability in initial conditions. IDT indicators include the pressure signal or various species from laser absorption diagnostics. Definitions of IDT include the peak, time of the maximum rate of change, or extrapolating the maximum slope to the zero signal level of the chosen indicator [18]. In this work, the OH* chemiluminescence collected in the *images* was used for defining the IDT.

In the case presented in Fig. 3, significant (>.01 normalized average image signal) OH* chemiluminescence was observed in the image at the time of the first vertical line, before indication of ignition was observed in either the pressure transducer signal or the traditional OH* emission diagnostic (both located 2 cm from the end-wall). The CRVST is generally employed under conditions where pressure increases are minimal, thereby facilitating reaction modeling. Here, higher fuel concentrations and reaction temperatures were intentionally chosen to emphasize inhomogeneous effects and pressure variations.

Figure 4 shows three sequential images collected at 12 kHz (inter-frame time of .083 ms) for the test reported in Fig. 3. A video is available in the supplementary material that contains additional images collected for the test depicted in Figs. 3 and 4.

In the first image ($t = 1.34$ ms) of Fig. 4, initial OH* chemiluminescence was observed near the walls of the shock tube (indicated by the white outline). Ignition in the core was evidenced in the second image ($t = 1.43$ ms), and ignition was evident everywhere within the shock tube cross section by the time of the third image ($t = 1.51$ ms).

Using the timing of the images and known characteristics of the combustion event, a semiquantitative estimate of the homogeneity within the shock tube was made. Equation 1 expresses the exponential temperature dependence of the IDT in an Arrhenius-like form. The relationship between the variation (a measure of uncertainty) in the IDT and the variation in temperature is shown in Eq. 2 where A is the pre-exponential factor, E_a is the activation energy, R is the universal gas constant and T is the temperature. Depending on the IDT correlation, the pre-exponential factor can be expressed as a function of multiple experimental variables (e.g., pressure, oxygen concentration and equivalence ratio) [19].

$$\tau_{\text{ign}} = A \exp\left(\frac{E_a}{RT}\right) \tag{1}$$

$$\frac{\Delta \tau_{\text{ign}}}{\tau_{\text{ign}}} = \left(\frac{-E_a}{RT}\right)\left(\frac{\Delta T}{T}\right) \tag{2}$$

Using Eq. 2 and the assumption that the pressure was uniform throughout the test volume, the spatial variation in temperature was estimated from the variation of the IDT throughout the test section. The key assumption here was
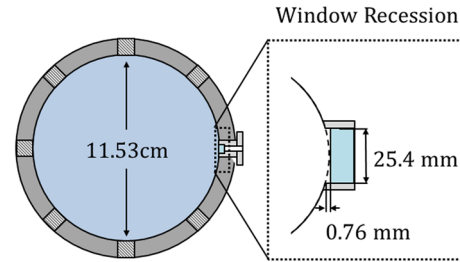

Fig. 5 Port locations are equally spaced circumferentially at an axial distance of 2 cm from the end-wall in the Stanford CRVST. The 0.76 mm recession caused by the window is exaggerated in the drawing. The plug that houses the flat window has the same contour as the shock tube wall

that the pockets of gas within the reaction volume ignited at different times due to the slight temperature differences. Though this was a simplistic assumption, it was nevertheless useful for initial quantification of the temperature variation.

The variation in the IDT throughout the shock tube was estimated as the time interval between the first image with significant OH* chemiluminescence ($t = 1.34$ ms) and the core ignition event with the maximum OH* chemiluminescence ($t = 1.51$ ms). This corresponded to a value of $\Delta \tau_{\text{ign}} = 0.17$ ms. Using Eq. 2 and $E_a = 186.6$ kJ/mol (44.6 kcal/mol) for *n*-heptane, a value of $\Delta T = 6.7$ K was obtained [19]. This estimate indicated that the temperature variation throughout the test section was around 0.5 % for this case.

3.2 Shock tube wall defects

To implement laser absorption and emission diagnostics in the Stanford CRVST, windows are placed in machined ports located 2 cm from the end-wall. There are eight ports equally spaced around the shock tube circumference, which can be filled with smoothly contoured plugs or plugs containing windows. When windows are installed, a 0.76 mm recession is created in the wall at the top and bottom of the window surface (Fig. 5).

These recessions may cause spatial temperature non-uniformities due to interactions with the incident and reflected shock waves. To test this hypothesis, window plugs were installed at different circumferential locations during ignition experiments. Indeed, reactions localized to the windows were observed, as shown in Fig. 6. Initial flames formed at the location of the window, in addition to other locations (some seemed to correspond to locations of smooth plugs, i.e., plugs without windows) along the shock tube wall. A magnified color scale was used to display the first image of the sequence to highlight the location of the initial flames.

Fig. 6 The effects of the window location, evolving over time, were recorded at 33 kHz with 4 µs exposure time for the combustion of *n*-heptane (21 % O$_2$/Ar, $\phi = 0.5$). The first image of each sequence has a magnified color scale to highlight the location of the initial flames. The initial reflected shock temperature and pressure along with the window location (*black rectangle*) were labeled for both experiments. A *white outline* was included to mark the location of the shock tube wall
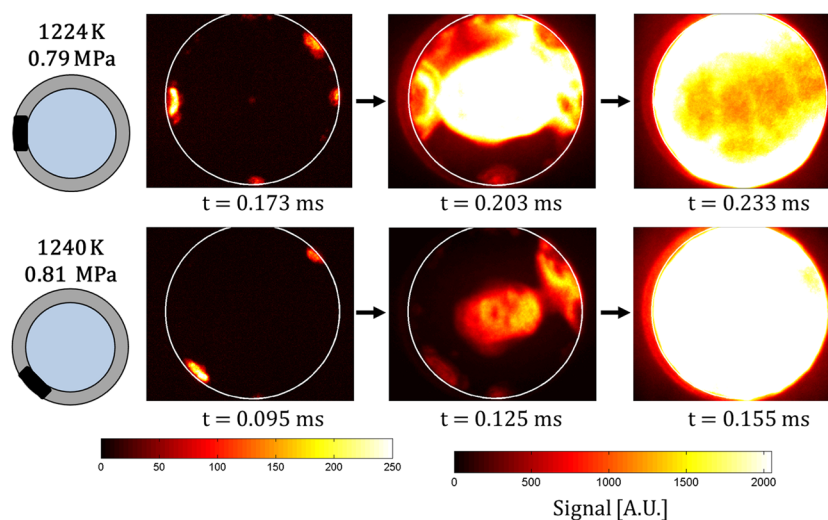
These findings demonstrated that the small recession in a window plug can be sufficient to promote initial local reactions. However, ignition in the core seemed unaffected. The flames that formed on the wall did not propagate to the core before the main ignition event. Nonetheless, it is important to recognize the possibility of local reactions near windows when implementing line-of-sight absorption or emission diagnostics. This could lead to a bias toward shorter measured ignition delay times by those diagnostics and could be an explanation for the early rise in OH* emission diagnostic seen in Fig. 3a for the previous case study.

3.3 Shock tube cleanliness

After three to five experiments in the shock tube, particulate can accumulate near the end-wall of the shock tube. Procedures for cleaning the shock tube have been developed to minimize the potential effects of these particulates. The CRVST was cleaned between experiments by brushing out and cleaning the last 2 m length near the end-wall with acetone before mechanically pumping the shock tube to a pressure of <0.1 Pa. The efficacy of the cleaning methodology was investigated by imaging the combustion event after the shock tube *was not* cleaned.

Figure 7a shows two different combustion events that took place after the shock tube *was not* cleaned for multiple runs (the shock tube was always pumped down between runs). Bright spots were seen that likely result from the small particulates that accumulated at the bottom of the shock tube. Many seemingly independent flames were observed to initiate in the bottom of the shock tube.

Figure 7b shows preignition images from tests after the shock tube *was* cleaned at similar initial reflected shock temperatures and pressures. The reaction zones were distributed circumferentially for both tests, in contrast to the tests conducted with particulates present.
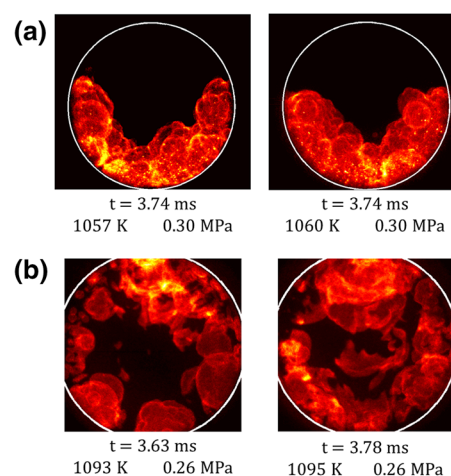

Fig. 7 a The combustion of *n*-heptane (21 % O$_2$/Ar, $\phi = 0.5$), after the shock tube *was not* cleaned, was recorded at 10 kHz with 5 µs exposure time. The *left* image was acquired after three experiments were performed *without* cleaning, and the *right* image was acquired after four experiments were performed *without* cleaning. **b** The combustion of *n*-heptane (21 % O$_2$/Ar, $\phi = 0.5$), after the last 2 m of the shock tube *was* cleaned, was recorded at 12 kHz with 5 µs exposure time. The initial reflected shock temperatures and pressures were labeled for each experiment. A *white outline* was included to mark the location of the shock tube wall

It is important to mention that for the other case studies presented previously, the shock tube was cleaned before each run. Confirming that an unclean shock tube changes the qualitative structure of preignition reactions was not surprising, but was a reminder that careful control of experimental variables is needed to achieve homogeneous or near-homogeneous combustion in reflected shock experiments. End-wall imaging has the potential to be a valuable tool for validating other aspects of shock tube performance and for facilitating further development of best practices for shock tube operation.

4 Conclusion

High-speed end-wall imaging of OH* chemilumines-cence was shown to be a powerful tool for understanding time-resolved, spatial details about shock tube kinetics experiments. The end-wall window provides new access for imaging of the structure and location of the earliest reaction zones in the shock tube, as well as the temporal development.

Three case studies that illustrated the utility of the tech-nique were presented. An estimate of the temperature vari-ability throughout the test section was found to be around 0.5 % for the test condition presented (n-heptane, 21 % O_2 /Ar, $\phi = 0.5$). The window recessions were found to cause initial flames to form at the window location. The impor-tance of routine shock tube cleaning was also demonstrated.

References

1. W. Bleakney, D.K. Weimer, C.H. Fletcher, The shock tube: a facility for investigations in fluid dynamics. Rev. Sci. Instrum. **20**(11), 807–815 (1949)
2. R.K. Hanson, D.F. Davidson, Recent advances in laser absorp-tion and shock tube methods for studies of combustion chemis-try. Prog. Energy Combust. Sci. **44**, 103–114 (2014)
3. D.J. Vermeer, J.W. Meyer, A.K. Oppenheim, Auto-ignition of hydrocarbons behind reflected shock waves. Combust. Flame **18**, 327–336 (1972)
4. K. Fieweger, R. Blumenthal, G. Adomeit, Self-ignition of S.I. engine model fuels: a shock tube investigation at high pressure. Combust. Flame **109**(4), 599–619 (1997)
5. J. Herzler, L. Jerig, P. Roth, Shock-tube study of the ignition of propane at intermediate temperatures and high pressures. Com-bust. Sci. Technol. **176**(10), 1627–1637 (2004)
6. O.G. Penyazkov, K.L. Sevrouk, V. Tangirala, N. Joshi, High-pressure ethylene oxidation behind reflected shock waves. Proc. Combust. Inst. **32**(2), 2421–2428 (2009)
7. K.A. Heufer, H. Olivier, S.P. Medvedev, S.V. Khomik, Optical investigation of shock induced ignition of different biofuels. in Proceedings of the 23rd ICDERS, University of California, Irvine, CA, 24–29 July 2011
8. J. Yoo, D. Mitchell, D.F. Davidson, R.K. Hanson, Planar laser-induced fluorescence imaging in shock tube flows. Exp. Fluids **49**, 751–759 (2010)
9. M. Wegener, M. Sutcliffe, R. Morgan, Optical study of a light diaphragm rupture process in an expansion tube. Shock Waves **10**, 167–178 (2000)
10. A.B. Mansfield, M.S. Wooldridge, H. Di, X. He, Low-tempera-ture ignition behavior of iso-octane. Fuel **139**, 79–86 (2015)
11. B.D. Stojkovic, T.D. Fansler, M.C. Drake, V. Sick, High-speed imaging of OH* and soot temperature and concentration in a stratified-charge direct-injection gasoline engine. Proc. Combust. Inst. **30**, 2657–2665 (2005)
12. V. Nori, J. Seitzman, Evaluation of chemiluminescence as a com-bustion diagnostic under varying operating conditions. in 46th AIAA Aerospace Sciences Meeting and Exhibit, Reno, Nevada, 7–10 Jan 2008
13. C.T. Bowan, D.J. Seery, Chemiluminescence in the high-temper-ature oxidation of methane. Combust. Flame **12**, 611–614 (1968)
14. H.N. Najm, P.H. Paul, C.J. Mueller, P.S. Wyckoff, On the ade-quacy of certain experimental observables as measurements of flame burning rate. Combust. Flame **113**, 312–332 (1998)
15. M.F. Campbell, A.M. Tulgestke, D.F. Davidson, R.K. Hanson, A second-generation constrained reaction volume shock tube. Rev. Sci. Instrum. **85**, 055108 (2014)
16. M.F. Campbell, T. Parise, A.M. Tulgestke, R.M. Spearrin, D.F. Davidson, R.K. Hanson, Strategies for obtaining long constant-pressure test times in shock tubes. Shock Waves **25**(6), 651–665 (2015)
17. M.F. Campbell, Studies of biodiesel surrogates using novel shock tube techniques. Ph.D. Thesis, Stanford University (2014)
18. D.F. Davidson, R.K. Hanson, Interpreting shock tube ignition data. Int. J. Chem. Kinet. **36**, 510–523 (2004)
19. D.C. Horning, D.F. Davidson, R.K. Hanson, Study of the high-temperature autoignition of n-Alkane/O_2/Ar mixtures. J. Pro-puls. Power **18**(2), 363–371 (2002)